

ASIC and ENaC type sodium channels: conformational states and the structures of the ion selectivity filters

Israel Hanukoglu

Laboratory of Cell Biology, Ariel University, Israel

Keywords

acid-sensing ion channels; conformational changes; epithelial sodium channels; hydrated ions; ion channels; protein dynamics; protein structure

Correspondence

I. Hanukoglu, Laboratory of Cell Biology, Ariel University, Ariel 40700 Israel
Tel: +972 3 9066293
E-mail: mbiochem@gmail.com

(Received 17 June 2016, revised 4 August 2016, accepted 26 August 2016)

doi:10.1111/febs.13840

The acid-sensing ion channels (ASICs) and epithelial sodium channels (ENaC) are members of a superfamily of channels that play critical roles in mechanosensation, chemosensation, nociception, and regulation of blood volume and pressure. These channels look and function like a tripartite funnel that directs the flow of Na^+ ions into the cytoplasm via the channel pore in the membrane. The subunits that form these channels share a common structure with two transmembrane segments (TM1 and TM2) and a large extracellular part. In most vertebrates, there are five paralogous genes that code for ASICs (ASIC1–ASIC5), and four for ENaC subunits alpha, beta, gamma, and delta (α , β , γ , and δ). While ASICs can form functional channels as a homo- or heterotrimer, ENaC functions as an obligate heterotrimer composed of α - β - γ or β - γ - δ subunits. The structure of ASIC has been determined in several conformations, including desensitized and open states. This review presents a comparison of the structures of these states using easy-to-understand molecular models of the full complex, the central tunnel that includes an outer vestibule, the channel pore, and ion selectivity filter. The differences in the secondary, tertiary, and quaternary structures of the states are summarized to pinpoint the conformational changes responsible for channel opening. Results of site-directed mutagenesis studies of ENaC subunits are examined in light of ASIC1 models. Based on these comparisons, a molecular model for the selectivity filter of ENaC is built by *in silico* mutagenesis of an ASIC1 structure. These models suggest that Na^+ ions pass through the filter in a hydrated state.

Introduction

Acid-sensing ion channels (ASICs) are proton (H^+)-activated sodium channels [1]. In the human genome, there are five paralogous ASIC genes that have been assigned the symbols of ASIC1, ASIC2, ASIC3, ASIC4, and ASIC5 [2–7] (Table 1). The proteins encoded by these genes represent subunits that form trimeric ion channels composed of either identical (homotrimeric) or different (heterotrimeric) subunits [1,8]. The five human ASIC subunits share 17–64% sequence identity. ASIC5 is the most divergent member of the

family and it forms an ion channel that is insensitive to protons but is sensitive to bile acids. Therefore, it was named as bile acid-sensitive ion channel (BASIC) (Table 1) [9,10]. Homologs of ASICs are also found in chordates and early vertebrates such as lamprey and shark, but in contrast to most mammalian homologs, these appear to be insensitive to protons [11,12].

In addition to ASICs, the human genome also includes four other homologous genes named SCNN1A, SCNN1B, SCNN1D, and SCNN1G [13–17]. The second

Abbreviations

ASIC, acid-sensing ion channel; ENaC, epithelial Na^+ channel; P_o , open probability; TM, transmembrane domain.

Table 1. Recommended and commonly used names of ASIC and ENaC paralogs in the human genome.

Gene name ^a	Protein Name ^b	Short name ^b	Other names
ASIC1	Acid-sensing ion channel 1	ASIC1	BNaC2
ASIC2	Acid-sensing ion channel 2	ASIC2	ASIC2a, BNC1, BNaC1, MDEG
ASIC3	Acid-sensing ion channel 3	ASIC3	TNaC1, DRASIC
ASIC4	Acid-sensing ion channel 4	ASIC4	BNaC4
ASIC5	Acid-sensing ion channel 5	ASIC5	INaC, BASIC
SCNN1A	Epithelial sodium channel alpha subunit	alpha-ENaC, ENaCA	
SCNN1B	Epithelial sodium channel beta subunit	beta-ENaC, ENaCB	
SCNN1G	Epithelial sodium channel gamma subunit	gamma-ENaC, ENaCG	
SCNN1D	Epithelial sodium channel delta subunit	delta ENaC, ENaCD	

^a Recommended by the HUGO Gene Nomenclature Committee. Previous gene names for ASIC paralogs 1–5 were ACCN2, ACCN1, ACCN3, ACCN4, and ACCN5.

^b Recommended by the UniProt database.

In some articles, the species is noted by the addition of a single letter prefix. Examples: rBASIC and hENaC for proteins from rat and human, respectively. The products of alternative mRNA splicing variants are specified by the addition of a single letter suffix. Examples: ASIC1a and ASIC1b.

N in the abbreviation SCNN1 was appended to mark that these genes code for nonvoltage-gated sodium channels. The proteins encoded by these genes represent a separate family named as epithelial sodium channel (ENaC) family (Table 1). The human ENaC subunits share 23–34% sequence identity among themselves and < 20% identity with ASIC subunits [18]. In contrast to ASICs that can form functional homotrimers, ENaC activity can be reconstituted fully only as a heterotrimer with an $\alpha\beta\gamma$ or a $\delta\beta\gamma$ composition [17,19]. However, only mutations in the alpha, beta, and gamma subunit genes lead to a hereditary disease characterized by severe salt wasting named as multisystem pseudohypoaldosteronism type I [18,20,21].

Analysis of the phylogeny of the ENaC subunits traced the origin of these proteins to early vertebrates but no direct ancestor could be identified in invertebrate genomes [18]. However, there are numerous homologous proteins in invertebrates that represent distinct families within the much larger ENaC/degenerin superfamily [18,22–24].

ASICs are mainly expressed in the central and peripheral nervous system, bone marrow, and gastrointestinal tract [7,25]. Gene knockout studies have revealed that the ASIC gene products are involved in diverse neural functions including synaptic plasticity, mechanosensation, chemosensation, and perception of pain (nociception) [7]. In contrast to ASICs, ENaC subunits are expressed mostly in salt absorbing epithelia with highest levels in the kidney, lung, colon, and parts of the male and female reproductive tracts [18,26,27]. The major functions of ENaC include Na⁺ reabsorption across high-resistance epithelia to maintain body salt and water homeostasis, regulation of

extracellular fluid (ECF) volume and blood pressure (mainly in the kidney) [28], regulation of airway surface liquid volume, and regulation of ciliary transport of gametes in the reproductive tract [18].

Both ASICs and ENaC are channels specific for sodium ions. However, their functions differ in many characteristics such as gating, ion selectivity, and response rates. ASICs and ENaC are also highly permeable to Li⁺ ions that are smaller than Na⁺ (Table 2) [1,29,30]. Under physiological conditions, lithium is present as a trace element [31]. In cases where lithium salts are used as a drug for the treatment of bipolar affective disorder, the therapeutic serum level is 0.5–1.0 mmol·L⁻¹ [32]. In the extracellular and intracellular fluids, Na⁺ and K⁺ ions are present at much higher concentrations: 140–150 mM, respectively. Thus, Li⁺ ions do not represent a competitor for sodium ions. However, at pharmacological doses, it is likely that Li⁺ ions also pass through ASIC- and ENaC-type channels.

Table 2. Radii of alkali metal ions, with and without a surrounding water shell (hydrated form).

Atom	Atomic radius (Å)	Ionic radius ^a (Å)	Mean hydrated ion radius ^a (Å)	Hydration number (Coordination number)
Li	1.45	0.60	3.40	4
Na	1.80	1.02–1.07	3.80	5–6
K	2.20	1.38–1.46	4.17	6–7
Rb	2.35	~1.64		8
Cs	2.60	~1.73		8

Mean diameter of a water molecule was taken as 2.8 Å.

^a Source: [93].

This review focuses on comparisons of ASIC1 and ENaC structure and function around the issues of the structures of the central pore and the ion selectivity filter of the channels. After a summary of functional comparisons between ASICs and ENaC, structural models of ASIC1 are presented. Previous results of ENaC site-directed mutagenesis studies are examined in light of ASIC1 models. These comparisons strengthen the view that the selectivity filter of ENaC is shaped by residues in the TM2 homologous to ASIC1 and that the changes in the conformation of the TM segments influence the opening of the channels. The comparisons of the states of channels are illustrated by easy-to-understand molecular models.

Functional comparisons of ASICs and ENaC

ASICs have been named as ‘acid-sensing ion channels’ because their pores are opened to the passage of ions in response to a rapid decrease in the pH of the environment. In the central and peripheral nervous systems, wherein ASICs are located, protons (H⁺) are released both during normal synaptic transmission, and various physiologic and pathologic events that lead to acidosis [1]. As activation of ASICs is dependent on the binding of protons to the channel subunits, ASICs have also been called as proton-gated channels [1].

Figure 1 shows an example profile of activation of rat ASIC1 in *Xenopus* oocytes by stepwise reduction of the pH of the bath solution. At pH 7.4, the whole-cell current remains stable and unchanged. Changing the bath buffer to pH 6.7 generates a small inward current that declines as rapidly as it is generated (Fig. 1). After the current drops to the initial level, the buffer is changed back to pH 7.4 for ~30 s. At the next step, the buffer is changed to a pH lower than the previous step (Fig. 1). At each step of bath pH reduction, the magnitude of the inward current increases up to pH 5.1, but still the current immediately drops as rapidly as it increases (Fig. 1). This type of assays of conductivity using stepwise reduction of pH has been used to measure some kinetic parameters of ASIC association with protons. For example, in the experiment in Fig. 1, half-maximal activation of ASIC1 is observed at pH 6.5, and maximal activation is achieved at pH 5.1. The pH for half-maximal activation (pH₅₀) reflects the affinity of ASIC for protons (i.e., the lower the value of pH₅₀, the lower the affinity; in other words, the lower the concentration of protons needed for activation, the higher is the affinity of ASIC for protons). The value of pH₅₀ for ASICs in

mammals varies between 4.8 and 6.7 [1,33–35]. In *Xenopus*, ASIC1 was found to have a higher pH₅₀ of 7.0 that has been ascribed to the physiology of the frog that has a higher arterial pH [36]. It should be noted that precise estimation of these values requires rapid exchange of bath solution to expose the channels to the full concentration of protons. Slow exchange of solution may result in the determination of artifactually lower pH₅₀ values (i.e., higher proton concentrations) necessary for activation [37].

The profile of pH-dependent current increase and subsequent decrease has led to the understanding that ASICs have at least three conformational states: (a) A closed state at physiological pH; (b) An open state initiated by proton binding, as a consequence of solution acidification; and (c) A desensitized state initiated by the continuous presence of protons. The closed state is distinct from the desensitized state, because in the closed state (but not in the desensitized state), the channel can be activated by a reduction of pH. ASICs can recover from desensitization within a few seconds after returning to pH 7.4 (Fig. 1) [1]. Repeated activation and desensitization of rat ASIC1, but not of ASIC2 and ASIC3, induces a gradually decreasing response that was named tachyphylaxis [38,39].

The kinetics of proton activation and desensitization differ between ASIC isoforms and splice variants. Proton sensitivity of ASIC homologs is observed in fishes, but missing in jawless vertebrate lampreys [40] and chordates [12]. ASIC2b, that is a splice variant of ASIC2, is not activated by reduced pH [41].

In contrast to ASICs, ENaC is constitutively active, meaning that the Na⁺ ions flow through it without a requirement for an activating factor. Therefore, as shown in Fig. 1, in heterologous cell systems that express ENaC (e.g., *Xenopus* oocytes), the cells have to be maintained in a bath solution that contains amiloride to fully inhibit ENaC. Uninhibited ENaC would result in flooding of the cell with Na⁺ ions followed by water molecules that would move to maintain isotonicity. To assay ENaC activity, the bath solution is changed to a solution without amiloride. Immediately after changing the solution, inward current increases and remains high until the solution is changed again including amiloride (Fig. 1). Thus, while ASICs are transiently activated, ENaC remains fully active. In contrast to the three major states of ASICs noted above, ENaC has two major states: 1) Open and 2) Closed. The probability of ENaC being in the open state is called ENaC open probability (P_o) [42].

The fact that ENaC is constitutively active raises questions about the mechanisms of regulation of

as a trimer of three identical subunits that form a funnel-like structure (Fig. 2). In this structure with a central axis of symmetry, six hydrophobic α -helical segments (three TM1s and three TM2s belonging to the three subunits) are bundled together forming the base of the channel that holds the channel in the membrane.

The first ASIC1 structure (PDB: 2QTS) represented an inactive form of the channel. In 2009, a second crystal structure was reported with a conformation that showed minimal function (PDB: 4NYK) [54]. The dynamic transformations of ASIC1 between closed–open–desensitized states present a challenge to capture the channel at a specific conformation for structural analysis. Many peptides found in the venoms of various species, such as spiders and snakes, act by binding to ion channels. Such peptides may fix or stabilize a channel at a specific functional state and may thus facilitate its structural analysis at a specific conformation. Thus, venom toxin peptides have been commonly used in the study of structure and function of ion channels [55,56]. Chen *et al.* [57] had already shown that the tarantula toxin psalmotoxin 1 (PcTx1) increases the affinity of ASIC1 to protons, and binds to it with different affinities at specific states. In 2012, two independent groups reported the crystal structure of chicken ASIC1 in a complex with psalmotoxin. In both structures,

psalmotoxin was found to bind at the interface of two subunits [58,59].

In 2014, Bacongus *et al.* [60] reported the crystal structure of ASIC1 in a complex with a snake toxin that stabilizes ASIC1 in an open conformation (PDB: 4NTW) (Fig. 2). The structures of ASIC1 trimer in both open and desensitized states show the same secondary structural domains. These domains have been named as palm, knuckle, finger, and thumb domain in analogy to hand anatomy as shown in Fig. 3. The palm domain is composed of a β -sheet and the other domains listed are composed of α -helical segments. Next to the palm domain, there is an additional β -sheet structure that has been called a β -ball (as if the ball is inside the palm of the hand) [53]. To complete the analogy to hand anatomy, the loops that connect the palm domain to the TM helices are called the wrist domain.

Currently, there is no crystal structure for other isoforms of ASIC or for ENaC. Our knowledge on other channels homologous to ASIC1 is based mostly on analyses of the structure and function of mutated channels expressed in *Xenopus* oocytes. Prior to the elucidation of the ASIC1 structure, studies were carried out based on sequence-dependent structural predictions. As presented in the following sections of this review, the results of these early studies can now be understood better in light of the ASIC1 models. These

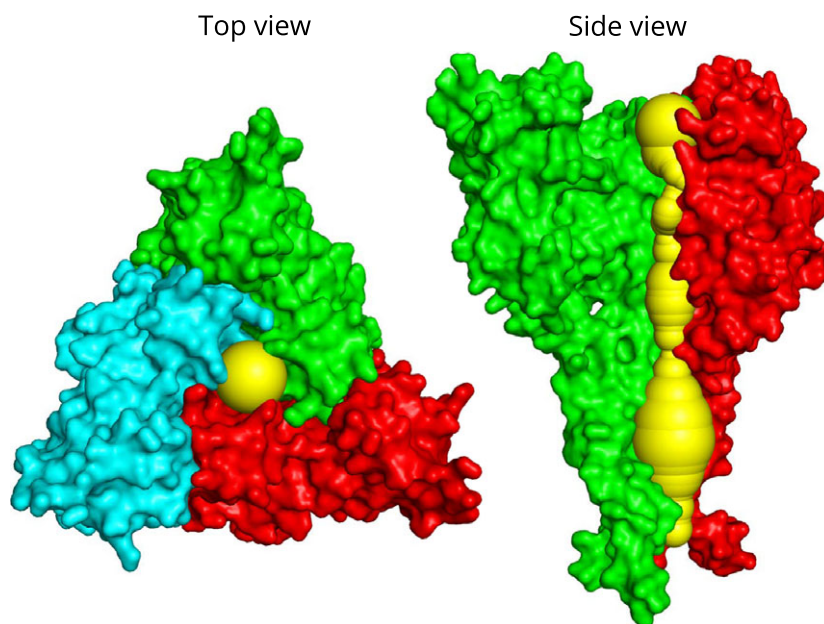


Fig. 2. The surface structure of ASIC1 trimer in the open conformation (PDB 4NTW). In the 'Top view', all three subunits are shown, each in a different color. In the 'Side view', only two subunits are shown to allow visualization of the tunnel in the center of the three subunits modeled using CHEXVIS software [63] (yellow colored). The snake toxin that was bound to ASIC1 is not shown [60].

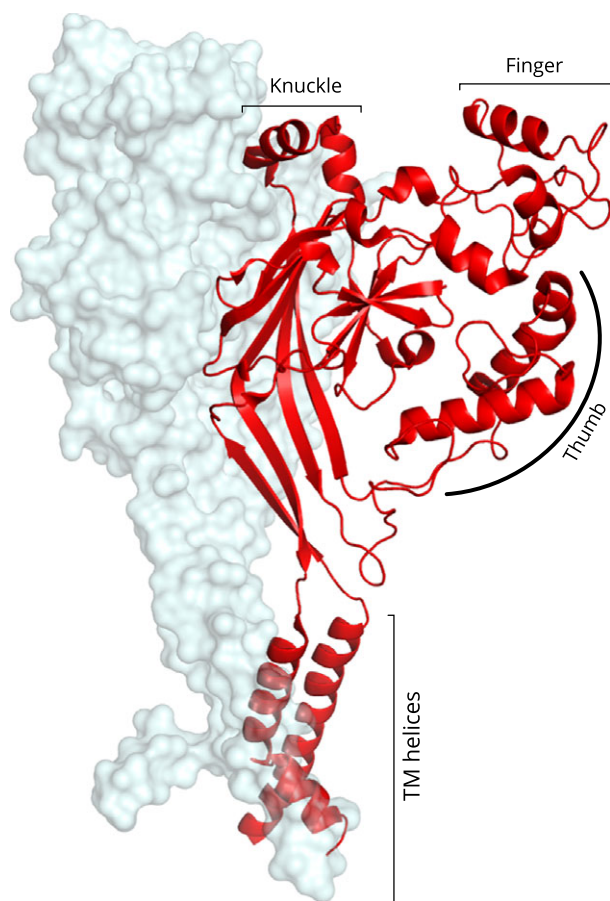


Fig. 3. The structures of the subunits A and B of ASIC1 (PDB 4NYK). The third subunit C is not shown to allow visibility of the other two subunits. For subunit A only the surface structure is shown in transparent form to allow visibility of the two TM helices of subunit B. The structure of subunit B is shown in cartoon mode to emphasize the secondary structural domains of the chain. Structural domains of ASIC1 were named as palm, knuckle, finger, and thumb in analogy to hand anatomy [53]. The orientation shown for the cartoon mode corresponds to left hand. The β -sheet at the interface between the subunits is the 'palm' domain (not marked) that is shown in greater detail in Fig. 6.

early studies greatly enhanced our understanding of the structure–function dynamics of the channels and the validity of their results is strengthened by their compatibility with the ASIC1 models. Yet, there is one issue where the elucidation of the ASIC1 structure contradicted some previous studies and that is the subunit stoichiometry of functional channels. Prior to the resolution of ASIC1 structure, several studies had suggested that ENaC may be assembled as a complex of 4–9 subunits (reviewed in [42]). The report on the trimeric structure of ASIC1 and subsequent modeling and experimental studies led to a consensus working

model that ENaC is also a trimer [8,18,42,61]. The validation of this model awaits the elucidation of a crystal structure for ENaC.

The central tunnel

The central axis of symmetry in between the three ASIC1 subunits contains a tunnel that runs from the extracellular top of the trimer to its bottom opening toward the cytoplasm [48,60] (Fig. 2). There are several software packages that have been designed to develop models of the channels/tunnels/pores in ion channels [62]. Baconguis *et al.* [60] have used the HOLE software to visualize the central tunnel in both desensitized and the open states of ASIC1. This tunnel runs in between the three subunits and it has constricted areas and large cavities that are called 'vestibules'. The shapes of these vestibules vary depending on the state of the channel [58,60] (Fig. 4).

For this review, I used a recent software named CHEXVIS to obtain a model of the central tunnel of ASIC1 [63]. The central tunnels modeled for the desensitized (4NYK) and the open-state (4NTW) structures are shown in Fig. 4. The outlines of both models are essentially the same as the models calculated by HOLE for the two states [60]. Yet, the CHEXVIS model of the central tunnel terminates at the narrowest part of the tunnel at the bottom that corresponds to the position of the selectivity filter ('GAS belt') (Fig. 4). The selectivity filter is followed by the intracellular vestibule (Fig. 4). The HOLE software model extends the tunnel further down to the end of the intracellular vestibule [60].

The most significant difference between the central tunnels of the two states of ASIC1 is that in the open state (4NTW), the area marked as the extracellular vestibule is vastly expanded relative to the desensitized state (4NYK) (Fig. 4). The lower half of the extracellular vestibule is located in between the TM helices, and the upper half is in the extracellular portion of the channel (Fig. 4). Thus, extracellular vestibule has also been called as the outer vestibule as it is open to the outside of the cell [64].

Fenestrations into the central tunnel

One of the most important questions about the function of these channels is the route(s) of flow of ions from the extracellular fluid into the central tunnel that ends with the opening of the pore at the cytoplasmic side. The largest openings (fenestrations) into the central tunnel are located in between the subunits at the level of the extracellular vestibule (Fig. 5). Because of the large size of these openings, the strongest flow of extracellular fluid

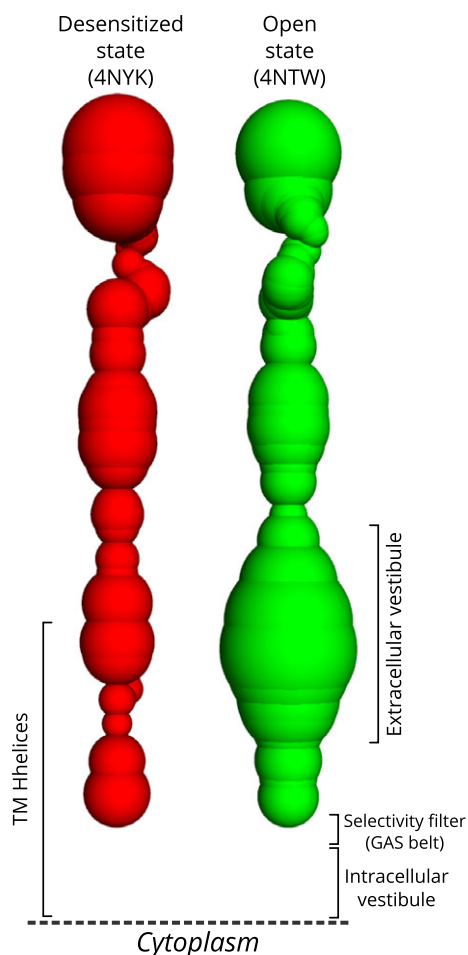


Fig. 4. The shapes of the central tunnel in the desensitized (4NYK) and open-state (4NTW) structures of ASIC1. The shapes of these two tunnels were modeled using CHEXVIS software [63]. The endpoint of the tunnel in the membrane was manually selected. The models were generated by PyMOL. Note that CHEXVIS tunnel terminates at the narrowest part of the tunnel at the bottom that corresponds to the position of the selectivity filter. CHEXVIS was programmed to end a tunnel after the last constriction when the radius of the pore monotonically increases. The structure of the intracellular vestibule matches these criteria; therefore it is not shown as part of the tunnel.

probably proceeds via these fenestrations into the extracellular vestibule and from there down to the pore of the channel located in the phospholipid bilayer in between the TM2 helices as noted below.

Channel pore at the end of the central tunnel

The pore of the ASIC1 channel, through which ions flow, starts close to the extracellular side of the phospholipid bilayer, and ends with an opening into the

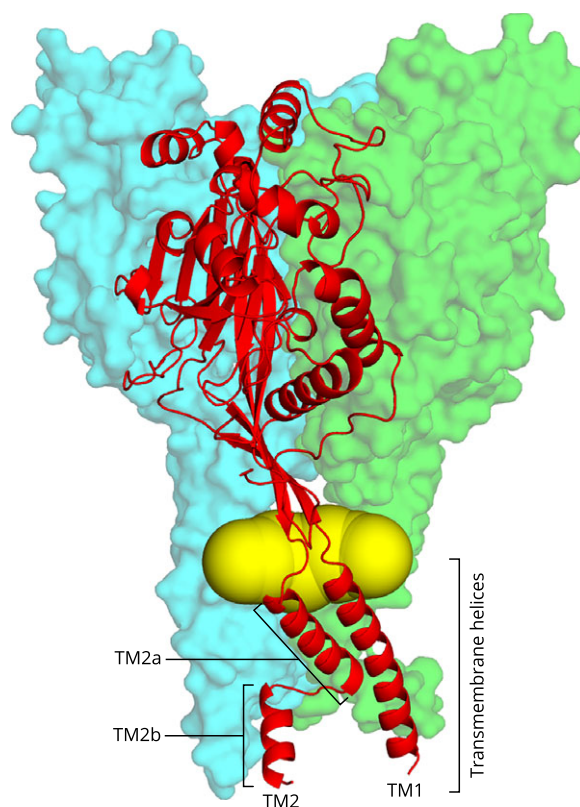


Fig. 5. The largest fenestrations (yellow colored) in-between the ASIC1 subunits in the open-state (4NTW). The fenestrations were modeled using CHEXVIS software [63]. Two of the subunits at the background are shown with their surfaces. The subunit at the front is shown in cartoon mode. Note that the yellow-colored fenestrations are located above the TM helices and merge into extracellular vestibule shown in Figs 2 and 4.

cytoplasm (Fig. 6). The three subunits that form a channel have six transmembrane segments: three TM1s and three TM2s as noted above. The pore of ASIC1 is formed by the three TM2s of the three subunits. The three TM2 helices are tightly juxtaposed forming a triangular structure, and the three TM1 helices are bound on the outside periphery of the TM2 bundle (Fig. 6). The pore of ASIC1 is located in the center of this TM2 bundle. In the desensitized conformation (left side of Fig. 6), the center is blocked, while in the open conformation (right side of Fig. 6), the center has an opening through which ions flow into the intracellular vestibule, and from there to the cytoplasm (Fig. 6).

The narrowest part of the pore is called the ‘selectivity filter’ as its function is to permit selective passage of ions. In ASIC1 and ENaC, the selectivity filter is located in between the TM2 segments [60,65].

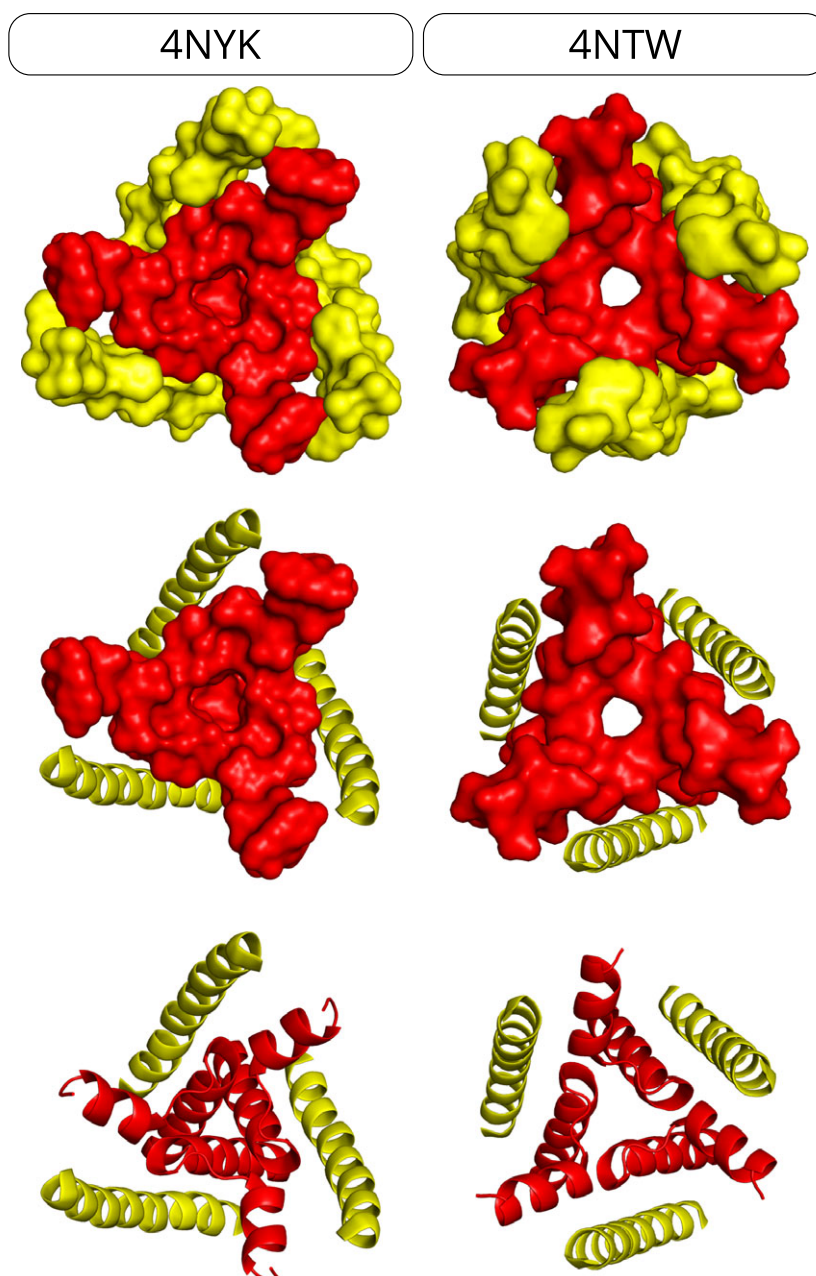


Fig. 6. The structure of the ion-pore of ASIC1 as viewed from the cytoplasmic side of the membrane. The left panel shows models for ASIC1 in the closed conformation (4NYK), and the right panel shows models for ASIC1 in the open conformation (4NTW). The top row of the two images shows the surfaces of TM1 (yellow) and TM2 (red) helices of the two conformations. In the middle row, the TM1 helices are shown in cartoon structure. The bottom row shows all six helices in cartoon mode. Note that only in the open conformation (4NTW), a pore is clearly visible at the center of the structure. The pore is surrounded by only three TM2 helices. The three TM1 helices are located at the periphery of the structure formed by the three TM2 helices.

Structural differences between conformational states

As noted above, ion conductivity of ASIC shows rapid changes that can be measured by electrophysiological

assays. The crystal structures of ASIC1 present a static picture at defined conditions from which it is difficult to deduce possible dynamic alterations. However, comparisons of ASIC structures in different functional states may allow identification of specific structural

changes associated with the functional differences. Hence, this section presents a comparison between two structures of ASIC1 that presumably represent its desensitized state (PDB 4NYK) [54] and the open state (PDB 4NWT) [60]. To compare the secondary, tertiary, and quaternary structures of the desensitized state (4NYK) and the open state (4NWT), these two structures were aligned using PyMol. The cartoon representations of these alignments are shown in Fig. 7. In the extracellular part of the two structures, the beta-ball, and the thumb domains are almost entirely superimposable. In the finger domain, two of three helices are superimposable. In the knuckle domain, the two helices are mostly overlapping (Fig. 7). In the palm domain, the β -strands in the upper part of the palm are superimposable, but in the lower part, short segments of the two β -strands connected to the TM helices are not superimposed and mark the beginning of the structural differences (see the lowest part of the palm domain in Fig. 7).

In contrast to the extracellular part, the transmembrane helices of the two states hardly overlap along their entire lengths (Fig. 7). This comparison reveals that the major conformational change between the desensitized and open conformations is in the orientation of the TM segments in the tertiary structure of the subunits.

The change in the orientation of the TM segments is also associated with a change in the quaternary structure of the trimer. In the open conformation, as compared to the desensitized state, the distance between the subunits significantly increases in the wrist region above the TM helices [60]. The first residue of the TM2 on the extracellular side, Glu426, can be taken as an index of this distance. In the desensitized state (4NYK), the distance between the C α atoms of Glu426 of the TM2s is 15.4 Å. In the open state (4NWT), this distance is increased by 8 Å to 23.4 Å. The expansion of the extracellular vestibule in the open state (Fig. 4) is one result of this change in the quaternary structure.

In contrast to the part embedded in the membrane, hardly any difference is observed in the intersubunit distance at the top of the channel. For example, the distance between the C α atoms of Asn144 (last residue of the α 2 helix in the finger domain) of the three subunits remains essentially the same in both states (62.7 versus 63.0 Å). Thus, the transformation between the two states appears to be associated with dynamic changes around the pore formed by the TMs.

The differences in the alignments of two short helices in the finger and knuckle domains indicate that these two domains have partial flexibility. They are both located in the peripheral regions of ASIC1 and may be involved in interaction with other molecules.

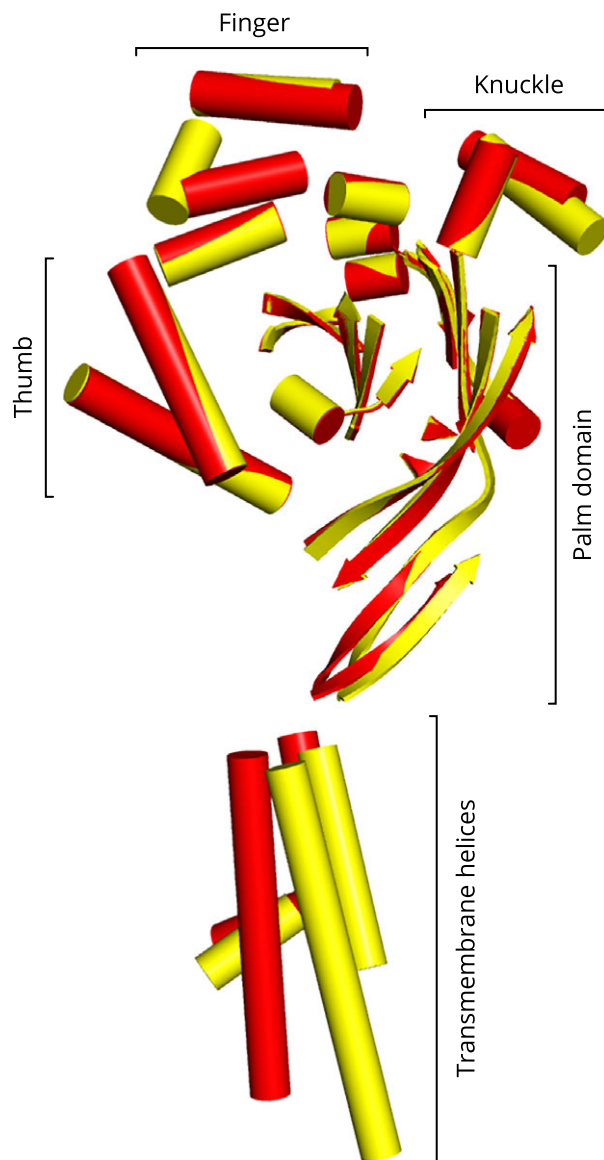


Fig. 7. Alignments of two ASIC1 structures: desensitized (PDB 4NYK, yellow colored) and open (PDB 4NWT, red colored) conformations. Only the α -helix (as a cylinder) and β -sheet (as a flat ribbon) structures are shown; the loops are not shown to simplify the image. The secondary structural domains (thumb, finger, knuckle, and palm domains) are marked separately. The two structures were aligned using PyMOL (version 1.7).

In two independent studies on ENaC, the knuckle domain was shown to be involved in sodium self-inhibition, suggesting that conformational changes here may affect channel function [48,66]. Moreover, the finger and knuckle domain sequences show high variability among members of the degenerin/ASIC/ENaC superfamily. It has been noted that these regions may be responsible for the functional specificity of the channels [22,23].

Who is pulling the strings of the TM segments?

In the extracellular part of ASIC, TM1 is connected to the $\beta 1$ strand, and TM2 is connected to the $\beta 12$ strand. Both of these strands form part of the palm domain β -sheet that is composed of seven strands (Fig. 8). The palm domains of the three subunits surround the central tunnel of the channel. Similar to the palm of the hand, the palm domain can be bent. The flexible parts of the palm domain that can be bent are the two loops that connect $\beta 1$ to $\beta 2$ and $\beta 11$ to $\beta 12$ strands. These loops are also called as the $\beta 1$ – $\beta 2$ linker and $\beta 11$ – $\beta 12$ linker. Part of the palm above these loops is known as the upper palm domain and the part below these loops is referred to as the lower palm [60,67].

In the open conformation of ASIC1, the bending (flexing) of the $\beta 11$ – $\beta 12$ loop affects two changes: the vestibule on the extracellular side of the membrane widens (see Fig. 4) and the $\beta 12$ strand is tilted, leading to a change in the angle of the TM2 helices and opening of the channel [60] (Fig. 6). Thus, a conformational change in the palm domains can affect two important aspects of the central tunnel: (a) constriction/expansion of the outer vestibule, and (b) the tilting of the TM helices that surround the pore of the channel [67].

Baconguis and Gouaux determined two crystal structures of PcTx1-bound ASIC1 with crystals grown at two pH values, high (pH 7.25) and low (pH 5.5). As noted above, these two conditions are associated with the nonconducting desensitized state, and with H⁺ activation, respectively. Comparison of these two structures led to the conclusions that the upper palm domain remains stable but the lower palm domain conformation shows major differences between the two conditions. These differences were ascribed to rearrangements in the conformations of residues located in the flexible $\beta 1$ – $\beta 2$ linker and the $\beta 11$ – $\beta 12$ linker [58].

Site-directed mutagenesis studies (carried out years before the report on the structure of ASIC1 in the open state) indeed showed that mutation of residues in the $\beta 1$ – $\beta 2$ and $\beta 11$ – $\beta 12$ linker regions strongly affect desensitization gating of ASIC1 [36,40,68].

The sequences of most of the strands in the palm domain are conserved across ASIC/ENaC families [18]. This raises the question of whether this domain plays a role in the gating of ENaC as in ASIC1. The sodium self-inhibition response of ENaC results in a reduction of the open probability of ENaC. This is a ligand-gating response similar to the proton desensitization of ASIC1 [45]. Alanine mutagenesis of charged residues in segments of ENaC subunits (homologous to the $\beta 12$ strand and the $\beta 11$ – $\beta 12$ linker regions of

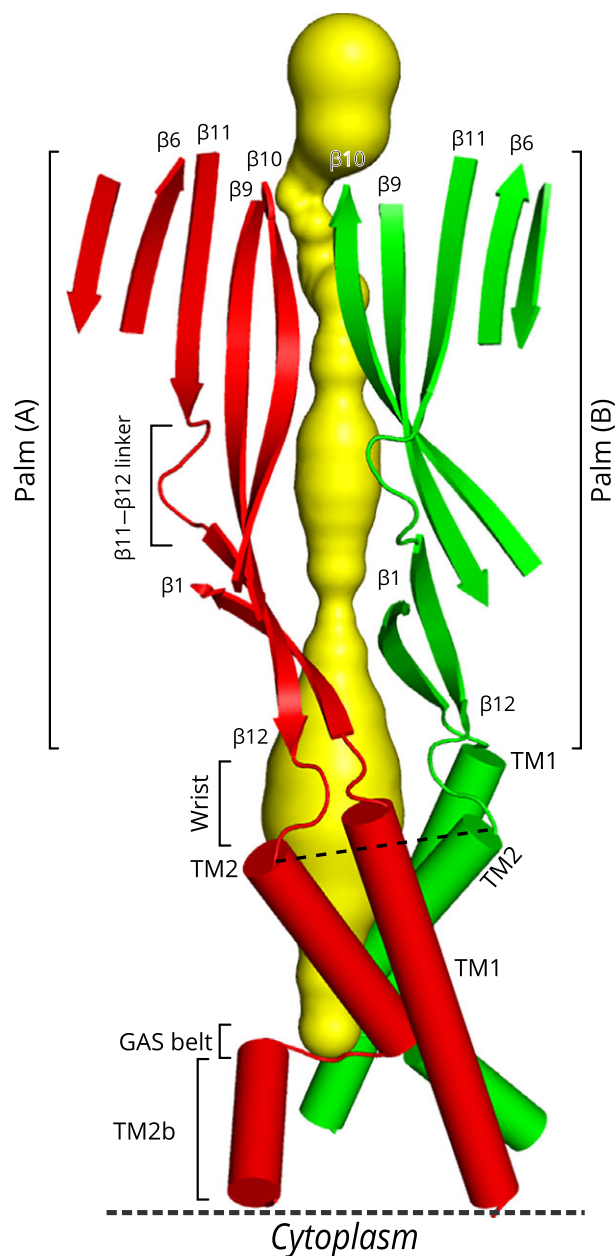


Fig. 8. The palm domains of subunits A and B of ASIC1 in the open conformation (4NTW) and the tunnel in the center of the trimer (see Fig. 2). The palm domain is composed of β -strands that make up a β -sheet [53]. In all three subunits, $\beta 1$ strand is connected to TM1 and $\beta 12$ strand is connected to TM2. Note that the palm domains are located at the interior part of the ASIC1 trimer, while knuckle, finger, and thumb domains are located at the periphery of the trimer (compare with Fig. 3). The third palm domain of subunit C (that is not shown) is located behind the central tunnel.

ASIC1) was also shown to decrease sodium self-inhibition response [48,69]. Thus, these studies provided evidence that segments of ENaC homologous to the $\beta 12$

strand and the β 11– β 12 linker play critical roles in channel gating similar to that in ASIC1.

The name ‘acid-sensing ion channel’ (ASIC) raises questions about where protons bind and how they activate ASIC. To answer such questions, most studies have employed site-directed mutagenesis of specific residues that have suspected roles based on the properties of the residues (such as the charge of the R-group) and their location in the resolved structure of ASIC1. In the first structure of ASIC1, Jasti *et al.* [53] had identified an acidic pocket between the finger and thumb domains. However, when Paukert *et al.* mutated six of the acidic residues (Asp and Glu) in this pocket of rat ASIC1 to Asn or Gln, they observed that none of these substitutions impaired H⁺-dependent activation. Altogether, Paukert *et al.* mutated 31 charged residues conserved in ASIC1–ASIC4 and observed that no single mutant blocked H⁺-dependent activation. Only triple mutants including Glu63 and Asp 78 eliminated proton gating [70]. It is possible that the mutants had no effect, because of the similarity of the mutated residues (Asp to Asn and Glu to Gln). A further examination of these residues by mutating them to Ala, thereby substituting just a methyl group instead of the charged group might have yielded different results. As noted above, ENaC has a sodium self-inhibition response that is a gating response similar to the desensitization of ASIC. We searched for residues responsible for this response by alanine mutagenesis of conserved charged residues in human ENaC subunits, and identified single residues whose mutagenesis reduced or eliminated the response [48,69]. It should be noted that these residues were located at the interface between subunits or in the central vestibule [48]. In such studies of site-directed mutagenesis, it is essential to include additional analyses to verify that the mutations have not caused general structural damage or inhibited cell surface expression of the channel.

Liechti *et al.* [71] systematically screened for charged residues that may be involved in proton binding and concluded that ASIC proton gating is dependent on protonation of many sites in ASIC. A study using computerized modeling has identified four pairs of residues (Asp238–Asp350, Glu220–Asp408, Glu239–Asp346, and Glu80–Glu417) as proton-binding sites of ASIC1 [72]. Two of these pairs are located in the palm domain, and the other two partly in the thumb domain. Schuhmacher *et al.* took a different approach to identify the segments of ASIC2 responsible for proton gating. As noted above, a splice variant of rat ASIC2 (named ASIC2b) was found to be

nonresponsive to pH drop. So, they attempted to identify to proton-sensitive segments by constructing chimeras between pH sensitive ASIC2a and insensitive ASIC2b and analyzing the responses of the chimeras. They concluded that large segments of the ASIC extracellular part are necessary to reinstate proton sensitivity [41].

In another innovative approach to identify the residues involved in proton gating, Li *et al.* examined the structure–function of lamprey ASIC1 that does not respond to protons. They showed that replacement of only two residues in the lamprey ASIC1 with residues found in the rat ASIC1 was sufficient to convert the lamprey ASIC1 into an H⁺-activated channel [40]. The full magnitude of response was achieved by the replacement of four residues with their rat counterparts: R64, H73, L77, and L85 (rat sequence numbering). As the authors point out, the fact that the proton activation response was reinstated by changing two nonionizable residues (L77 and L85), indicates the wild-type lamprey ASIC1 has a proton sensor, and that the substitutions reduced the rate of desensitization making the response detectable. Most importantly, the two residues that affected such drastic changes are located in the β 1-strand and β 1– β 2 linker region, the importance of which was noted above.

In 2009, two independent laboratories showed that mutations of strictly conserved residues Tyr72, Pro287, and Trp288 (numbering of the residues correspond to the ASIC1 structure) to Gly/Ala abolished the pH activation of ASIC1, raising the hypothesis that the aromatic pair is essential for proton-gating of ASICs [73,74]. To understand the effects of these mutations, the positions of the residues are shown in Fig. 9. Tyr72 is located at the end of TM1, and Pro287 and Trp288 are located in a beta-turn between the β 9-strand and the thumb domain that has two helices (Fig. 3). P287 and W288 in this β -turn are tethered to Y72 by interactions between the R-groups of the residues. Mutation of the aromatic residues to a residue with a nonaromatic R-group greatly reduced or abolished ASIC activation by a drop in pH. To examine whether the structure of this β -turn region undergoes changes, I superimposed the desensitized state (4NYK) and the open-state (4NWT) structures using three C α atoms of the three residues (Y72, P287, and W288) as tethers for superimposition using Discovery Studio Visualizer. In this comparison, the β -turn region, its conformation, and its distance from Tyr72 at the end of TM1 showed nearly identical positions. Thus, apparently this region does not show a change in these two states.

An alternative possibility for the effect of the nonaromatic mutations is that the mutations cause a major change in ASIC1 structure. Aromatic residues commonly appear in pairs in proteins and the π - π interactions between the R-groups of these residues are involved in the stabilization of tertiary and quaternary structures and inner core regions of proteins [75,76]. In the present case, the π -stacking is T-shaped that is a most favorable interaction. One of the studies did not examine if the mutations affected surface expression, and the second showed differences in surface expression relative to wild-type. A cursory examination of the ASIC1 structure (Fig. 9) suggests that the breakage of the π - π interactions between the end of TM1 (Y72) and the β -turn may adversely affect the thumb domain stability with general adverse consequences. Nonetheless, these extensive studies are important for drawing attention to the importance of the linkage between the TM1 and thumb domain which in turn is in contact with the finger domain.

The answer to the heading of this section ‘Who is pulling the strings of the TM segments?’ would not be complete without mentioning the intracellular segments (‘tails’) of ASIC and ENaC. The ASIC1 models are based on engineered constructs with partial N

and C termini connected to the TM1 and TM2 segments, respectively. Mutations of residues at the N and C termini of the TMs have demonstrated that these intracellular segments may also influence both the function and ion selectivity of ENaC [77]. Moreover, the movement of the N- and C-tails by intracellular factors and cytoskeletal elements may influence the conformation of the TM2 and hence the channel function [18,78].

The selectivity filters of ASIC and ENaC

The selectivity filter of an ion channel is the narrowest part of the channel pore through which ions pass selectively. The atomic and ionic radii of alkali metals increase with the atomic number: $\text{Li}^+ < \text{Na}^+ < \text{K}^+ < \text{Rb}^+ < \text{Cs}^+$ (Table 2). ASIC/ENaC family of channels are selective for Na^+ (ionic radius $\sim 1.0 \text{ \AA}$) over K^+ (ionic radius $\sim 1.5 \text{ \AA}$) [1,29,64]. The selectivity of ENaC is much higher than that of ASIC as the permeability ratio of Na^+/K^+ is > 100 for ENaC and in the range of 5–14 for ASICs [1]. This section summarizes our current knowledge on the selectivity filter of ASIC and ENaC subunits in separate subsections.

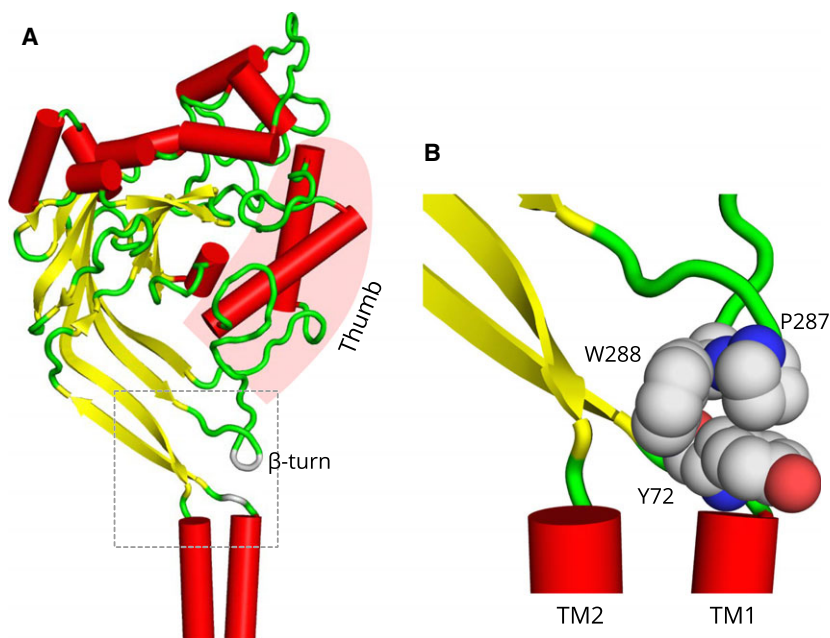


Fig. 9. The locations of the aromatic residues Tyr72 and Trp288 that connect between the C terminus of TM1 and the β -turn that is connected to the thumb domain. (A) A cartoon view of the 4NTW model of ASIC1. The square marks the area magnified in B. Note that the tethering of the β -turn to Tyr72 at the end of TM1 stabilizes the whole thumb domain. (B) Magnified view showing three residues in space-filling model. Note that Tyr72 aromatic ring is at the end of TM1. Trp288 is located at the side of Tyr72. This orientation of the two aromatic residues is called T-shaped conformation. Pro287 is on top of Tyr72. Colors: red, helix; yellow, sheet; and green, loop. Colors of atoms: gray, C; red, O; and blue, N.

Selectivity filter of ASIC1

In the open-state of ASIC1 (PDB 4NTW), the selectivity filter is located at the most constricted part, at the bottom of the outer vestibule [60] (Fig. 8). The recent structural models of ASIC1 trimer (4NYK and 4NTW) have revealed that TM2 is not a continuous helix; it is split into two parts (named as TM2a and TM2b) separated by a stretch of three residues (Gly443-Ala444-Ser445 in chicken ASIC1, abbreviated as GAS) that are in an extended configuration (Figs 5 and 8). Amazingly, the second part of the helix (TM2b) is positioned as an extension of the first part of the helix (TM2a) of the neighboring subunit. In other words, TM2a helix is spatially followed and extended by the TM2b helix of the neighboring subunit [60].

The selectivity filter of ASIC1 is formed by nine amino acid residues to which each subunit contributes three residues (G-A-S) that are in an extended configuration in between the two parts of TM2 (Fig. 10). In ASIC1 sequences from nearly all vertebrate species, the G-A-S sequence is strictly conserved. Baconguis *et al.* [60] have named this as the ‘GAS belt’ and GAS motif of ASIC1 and suggested that a similar discontinuous TM2 is present in other ASIC/ENaC family members.

In the GAS belt, the carbonyl oxygens of Gly443 of all three subunits face the pore (Fig. 10). Thus, these oxygens with negative potential contribute to the attraction of positively charged ions into the channel pore.

To complement the structural models of ASIC1, Li *et al.* identified the narrowest part of the channel by measuring the rates of modification of cysteines substituted for residues along the pore, using thiol-specific reagents. Based on their findings, they suggested that

D433 serves as the gate in the closed state, and G443 of the GAS belt is part of the selectivity filter in the open conformation [79].

Selectivity filter of ENaC

In each ENaC subunit, there is a strictly conserved tripeptide motif homologous to the ASIC1 G-A-S motif, but the sequences of the motifs differ between subunits. In the homologous region, the consensus sequence for the α , β , and γ ENaC subunits are GSS, GGS, and SCS, respectively. These sequences are 100% identical in 20 species that have been examined [18]. The delta ENaC subunit orthologs are less conserved and show two major variants in different species: GAS and GSS. To facilitate references to these consensus sequences, Table 3 presents the numbers for each amino acid of the consensus sequence for the three species that have been used in such studies. To visualize the selectivity filter of ENaC, I generated a model for the filter of ENaC by *in silico* mutagenesis of ASIC1 structure (Fig. 11). Despite the differences in the sequences, the structure of the ENaC selectivity filter in this model is highly similar to that of ASIC1 (Fig. 10). The different side chains of the residues project on the outer site of the selectivity filter. Because of the different consensus sequences, studies on each subunit are reviewed separately below:

α ENaC sequence GSS

The first comprehensive examination of the role of the conserved residues in the α ENaC pore was carried out

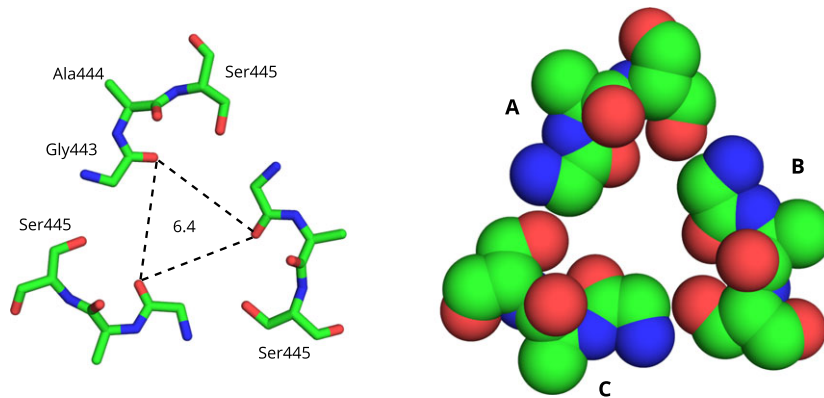


Fig. 10. The ‘GAS belt’ selectivity filter of chicken ASIC1 that is composed of Gly443, Ala444, and Ser445 of the three ASIC1 subunits (PDB 4NTW). Both the stick and CPK models show the top view from the extracellular side of the membrane. These three residues are located at the extended structure between the two parts of the TM2 (see Figs 4 and 7) [60]. Atom colors: C, green; N, blue; O, red. The dashed lines mark the distance between the carbonyl oxygen atoms of Gly443.

Table 3. The amino acid residue numbers for the conserved selectivity filter sequences of four ENaC subunits in commonly studied species.^a

ENaC subunit	α	β	γ	δ
Consensus	Gly-Ser-Ser	Gly-Gly-Ser	Ser-Cys-Ser	Gly-Ala-Ser
Human	G560-S561-S562	G531-G532-S533	S540-C541-S542	G537-A538-S539
Mouse	G587-S588-S589	G529-G530-S531	S546-C547-S548	–
Rat	G587-S588-S589	G529-G530-S531	S541-C542-S543	–

^a The homologous sequence in chicken ASIC1 is G443-A444-S445.

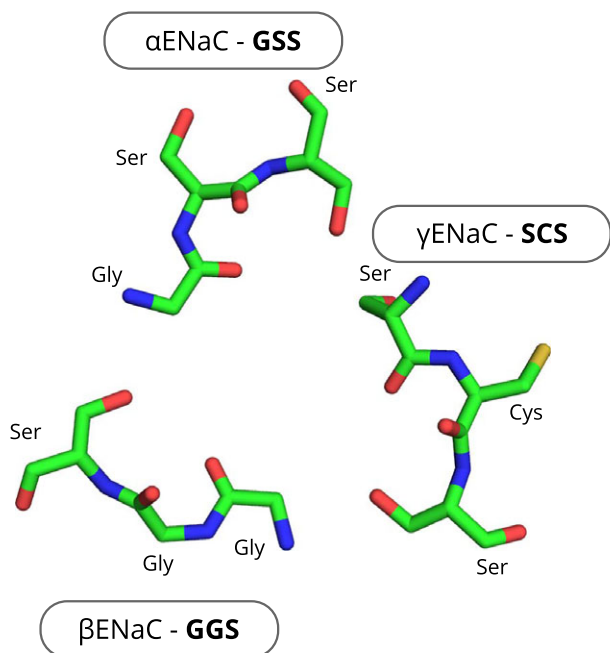


Fig. 11. A model for the selectivity filter of ENaC based on the ASIC1 structure (4NTW). This model was generated by *in silico* mutagenesis of ASIC1 filter (see Fig. 10), using PyMOL. The triad of residues indicated for each subunit is strictly conserved in vertebrates [18]. Atom colors: C, green; N, blue; O, red.

by [30]. They mutated the last Ser (S589) of the GSS motif of rat α ENaC to Ala, Cys, and Asp and expressed the mutated subunits with wild-type (WT) β and γ subunits. While the permeability ratio I_{K^+}/I_{Na^+} was 0.00 for the WT, for the S589A, S589C, and S589D mutants, this ratio increased to 0.06, 0.21, and 0.32, respectively. The authors suggested that substitutions of residues bigger than Ser enlarged ‘the pore at selectivity filter’ [30]. In a later study, they examined a greater number of mutants and suggested that α S589 side chain points ‘toward the interface between the subunits’ [65].

Sheng *et al.* [80,81] systematically mutated each of the residues from V569 to S592 in mouse α subunit to

Cys and observed that only α S589C mutation greatly increased permeability to K⁺ followed by G587C mutation that had a smaller effect. Thus, these studies established that the GSS motif of α ENaC (homologous to the GAS motif of ASIC1) forms part of the selectivity filter of ENaC.

The S589 residue of the mouse rat α ENaC is homologous to the S445 of chicken ASIC1. The R-group of S445 is at the edge of the GAS motif and is adjacent to the Gly of the GAS sequence in the neighboring subunit (Fig. 10). Increasing the size of the side chain of the residue located here would be expected to enlarge the ‘the pore at selectivity filter’ just as Kellenberger *et al.* correctly predicted [65].

It should be noted that mutation of α S589 to residues with side chains bigger than His (Leu, Met, Arg, Lys, Phe, and Trp) reduced ENaC activity to nondetectable levels, apparently as a result of a damage to the process of ENaC transport to the membrane [65]. Recently, we showed that alanine mutagenesis of conserved residues at the interface between ENaC subunits significantly reduces cell surface expression of ENaC [48,69]. As the rat α S589 is at subunit interface, substitution of large residues apparently prevents the formation of a trimeric complex between ENaC subunits that is a prerequisite for transport to the cell surface.

Mutation of the first residue of the GSS motif (rat α G587) to alanine did not change the permeability of rat ENaC to K⁺ ions [64]. In contrast, mutation of mouse G587 to Cys was observed to increase permeability to K⁺ [80]. The first residue of the motif is located at intersubunit interface (Fig. 10). These results suggest that the substitution of a residue with a side chain larger than Ala may affect the width of the filter and allow passage of bigger K⁺ ion.

Mutation of the second residue of the GSS motif (α S588) to Ala also did not change the permeability of rat ENaC to K⁺ ions [64]. As seen in Figs 10 and 11, the side chain of the Ala (a methyl group) in the GAS motif protrudes in a direction opposite to that of the center of the pore. Thus, mutation of this residue would not be expected to affect directly channel pore

size. The lack of an effect of these mutations indicates that similar to the ASIC1 structure, the side chains of these residues are not pointed in the direction of the pore. Yet, mutations of these two residues slightly reduced the permeability of Li⁺ relative to Na⁺ [64].

βENaC sequence GGS

The consensus sequence for the selectivity filter of βENaC is GGS in vertebrates [18]. Similar to the results with αENaC, mutation of the second Gly (in GGS) in mouse and rat βENaC (βG530) did not change permeability to K⁺ ions [64,82]. Mutation of the first Gly (βG529) to Ser or Cys significantly increased permeability to K⁺ ions [64,82]. Mutations of the residues before and after the βENaC consensus sequence GGS had no effect on K⁺ ion permeability [64], further strengthening the view that ASIC1 model applies to ENaC subunits as well (Fig. 11).

γENaC sequence SCS

The consensus sequence for the selectivity filter of γENaC is SCS in vertebrates [18]. In a mutagenesis study, Snyder *et al.* [83] mutated each of the residues in a long stretch from S519 to C545 of human γENaC. The only mutation that enhanced the permeability of K⁺ was S542C that is in a position homologous to S in the ASIC1 GAS motif. In addition, S540C mutation reduced the permeability of Li⁺ [83]. In studies with the rat γENaC, S541A and C542A mutations did not change the permeability to K⁺ [64].

In a different line, Fyfe *et al.* generated chimeric ENaC subunits combining parts of the rat α and β and γ and β subunits and replacing the TM2 and C termini of the subunits. These chimeric ENaCs exhibited different properties but were all impermeable to K⁺ ions [84].

δENaC sequence GAS/GSS

The delta ENaC subunit shows maximal activity when coexpressed together with the β and γ subunits [17]. Among vertebrates, the delta subunit sequences show greater interspecies variability, as compared to the α, β, and γ subunits. In primates (including humans, chimp, gorilla, orangutan, gibbon, and rhesus), the δ-ENaC selectivity filter motif is GAS (identical to ASIC), but in other vertebrate species, the most common motif is GSS. In Table 3, no sequence is listed for the mouse and rat because in the Muridae family of rodents the gene for the delta

subunit apparently has been lost in some species [18,85]. However, the genome sequences of other rodents such as the guinea pig and the mole rat have a δ-ENaC ortholog. The selectivity filter motif has not been examined by site-directed mutagenesis. In the human genome, there are several splice variants two of which has been extensively characterized [86,87]. The longer variant has an extra 66 residue segment at the N-terminal region. Within a trimer composition of δβγ, both forms are activated by external protons and have similar alkali ion selectivities [87].

The role of the DEG residue in ENaC and ASIC2

Over two decades ago, studies on the nematode *Caenorhabditis elegans* mutants indicated that the function of mechanosensitive ion channels is most strongly affected by mutations at the start of the TM2 segment of subunits encoded by *deg-1*, *mec-4*, and *mec-10* genes homologous to ASIC and ENaC families [24,88]. A dominant mutation that causes neuronal degeneration (Deg phenotype) in *C. elegans* was identified to be a result of Ala707 mutation to Val (A707V) in the *deg-1* gene [88]. The homologs of this residue (Ala707) in other members of ENaC/degenerin family is known as the DEG residue [18,89]. In ASIC1, the DEG residue is a glycine, but in all ENaC subunits, the homologous position has a serine [18]. A comprehensive study by Snyder *et al.* examined the role of the DEG residue in human ENaC subunits by mutagenesis and covalent modification of the residue. The results of this study indicated that the DEG residue increases the open probability (P_o) of ENaC but does not appear to be part of the selectivity filter, as mutation of the residue did not alter the selectivity of ENaC for Na⁺ [89]. Thus, they concluded that the DEG residue is located in the extracellular (outer) vestibule.

Similar to the effect on ENaC, the mutation of the DEG residue Gly430 in ASIC2 (MDEG) activated ASIC2, but in contrast to the effect in ENaC, greatly reduced the selectivity of the channel between Na⁺ and K⁺ [90,91].

The roles of the acidic residues in TM2

The distal part of the TM2 segments close to the cytoplasm includes three highly conserved acidic residues (Asp and Glu) in both ASICs and ENaC [18]. To examine the role of these residues, Langloh *et al.* mutated the three residues in human α-ENaC to basic residues (E568R, E571R, and D575R) and expressed

these in *Xenopus* oocytes together with wild-type β and γ subunits. They observed that amiloride-sensitive current was significantly reduced by the mutations but Na⁺/K⁺ permeability was not affected [92]. In the 4NTW model of ASIC1, the first Glu (E450) in chicken ASIC1 protrudes into the intracellular vestibule. If in ENaC, the homologous residue E568 has a similar position, then its mutation to a basic residue would indeed be expected to hinder the smooth flow of Na⁺ ions from the pore into the cytoplasm.

Na⁺ versus K⁺ selectivity in a hydrated state

As noted above, both ASIC and ENaC are selective for Na⁺ ions, though to different degrees (see the beginning of this section). In aqueous solutions, the alkali metal ions Li⁺, Na⁺, and K⁺ are surrounded by a shell of water molecules. The number of water molecules in a shell (called as the ‘hydration’ or ‘coordination’ number) ranges from 4 to 8 depending on the size of the alkali metal (Table 2) [93]. This raises a question whether the ions pass through the selectivity filter of channels enveloped within a hydration shell or in a dehydrated state as singular ions.

Molecular mechanisms of ion selectivity have been investigated extensively for voltage-gated sodium and potassium channels that are expressed in neurons and muscle cells and their prokaryotic homologs [94–100]. The main α -subunit of voltage-gated ion channels are composed of four domains (as in voltage-gated Na⁺ channel, Nav) or four homologous subunits (as in voltage-gated K⁺ channel, Kv, and in prokaryotic NavAb) [98,101–103]. These four domains or subunits have a common structure composed of six transmembrane segments that have been named as S1–S6 [101]. The first four TM segments (S1–S4) form the voltage sensing domain, and the channel pore is formed by the S5 and S6 segments in between which there is a loop called pore-loop or P-loop [101,102].

Despite the structural homology between the Na⁺ and K⁺ channels, the mechanisms of their ion selectivity are very different. The narrow selectivity filter of Kv is lined with oxygens of carbonyl and side-chain hydroxyl groups. The K⁺ ions that approach the mouth of this pore are drawn into it by the negative potential of the oxygens and pass through the narrow selectivity filter in a dehydrated state. The pore cannot accommodate hydrated ions and the ‘snug-fit’ (tight-fit) of the K⁺ ions in the pore is considered as one of the factors responsible for the selectivity for K⁺ over Na⁺ [96].

In contrast to K⁺ selective channels, the selectivity filter of the NavAb is large, and it is thought that

Na⁺ ions pass through it in a hydrated form [97,98,100]. Molecular dynamics simulations of NavAb indicate that hydrated K⁺ ions cannot fit through the narrow portion of the pore as a consequence of two properties of the pore, its size and the protruding charge of Glu177 [104]. Similarly, in contrast to Kv-type channels, the selectivity filters of ASIC and ENaC are large. The GAS motif of the ASIC selectivity filter outlines an equilateral triangle with a length of 6.4 Å per side and with carbonyl oxygens at the vertices (Fig. 10). This triangle defines a circumscribed circle (a circle which passes through all three vertices of a triangle) with a radius of 3.7 Å. Figure 12 presents a comparison of the sizes of hydrated Na⁺ and K⁺ ions. As previously noted [60], the estimated radius of hydrated Na⁺ ion (3.8 Å) could fit tightly into the ASIC GAS ‘belt’ but a hydrated K⁺ ion could not. Thus, it appears that the Na⁺ ions pass through the filter in a hydrated state. Moreover, in contrast to the K⁺ channels, in the ASIC structure, there does not appear to be a mechanism for the ‘dehydration’ or ‘desolvation’

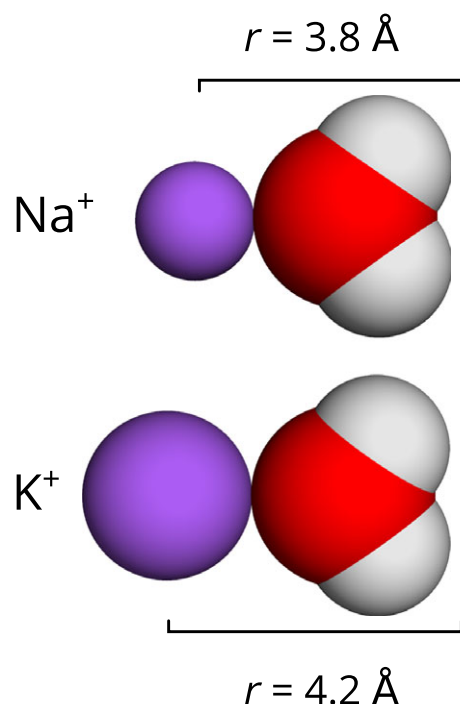


Fig. 12. Radii of hydrated Na⁺ and K⁺ ions. The figure shows only one molecule of water associated with the alkali metal ion. The number of water molecules that surround the ion can be 5 to 7 (see Table 2). Thus, the full diameter of the hydrated ion should be 2× the length of the radius shown for each ion. The mean diameter of water molecule was taken as 2.8 Å. Note that, in aqueous solution, the positively charged ions are associated with the oxygen atom that carries a negative potential.

of Na⁺ ions (i.e., stripping of the water molecules surrounding the Na⁺ ion), during their passage via the filter.

Lithium is the smallest alkali metal ion (Table 2). The permeability of ASIC and ENaC to Li⁺ is higher than Na⁺ [13,29,105,106]. Thus, the order of selectivity for alkali metal ions for ASIC and ENaC is Li⁺>Na⁺>>K⁺. Some authors have commented that this ion size-dependent order of permeability may be an indication that the channel selects ions based on the 'size of the completely dehydrated ion'. Yet, it should be noted that the sizes of both hydrated and dehydrated cations follow the same order: Li⁺<Na⁺<K⁺ (Table 2). With our current knowledge of the ASIC1 structure, it has been hypothesized that the pores of these channels have been shaped to allow passage of hydrated ions and not dehydrated ions [58,60].

As noted, ENaC is much more selective for Na⁺ as compared to K⁺. It is possible that this stringency reflects a tighter structure of the 'GAS belt' filter in ENaC as modeled in Fig. 11. The answer to this and many other questions about ENaC structure–function versus ASIC awaits the resolution of the crystal structure of ENaC.

Conclusions

The resolution of the crystal structures of ASIC1 trimer in desensitized and toxin-bound open forms has greatly increased our understanding of ASIC- as well as ENaC-type channels. This review presented a comparison of the structures of these states using easy-to-understand molecular models of the full complex, the central tunnel that includes an outer vestibule, the channel pore, and ion selectivity filter. The differences in the secondary, tertiary, and quaternary structures of these states were summarized to pinpoint the positions of conformational changes responsible for channel opening. In contrast to potassium channels wherein dehydrated K⁺ ions pass through a narrow selectivity filter, in ASIC, the filter is large and allows passage of hydrated Na⁺ ions but not larger hydrated K⁺ ions.

Studies on ENaC structure and function mainly by site-directed mutagenesis of conserved sequences provide solid evidence that the trimeric structure and the selectivity filter model of GAS belt of ASIC apply to ENaC as well. Much of the studies on ENaC selectivity and function were performed prior to the elucidation of the structure of ASIC. The results of earlier studies on the expression of mutagenized ENaC subunits were re-examined in light of ASIC1 structures. Based on these comparisons, a molecular model for

the selectivity filter of ENaC was built by *in silico* mutagenesis of an ASIC1 structure.

Many details about the structure and function of these channels still remain to be answered. These include the structural loci that are responsible for ionic regulation, conformational changes in the vestibules in the central tunnel, and molecular mechanisms of the gating of the channels. The studies reviewed here show a convergence of the results of independent approaches using crystallographic studies, and *in vitro* expression of mutated channels. The past achievements summarized here demonstrate that the combination of both static atomic structures and dynamic functional assays of especially mutated channel subunits are essential to advance our understanding of the functions of these channels.

Acknowledgements

I thank Girish Kumar Kaitholil for his careful reading of the manuscript.

References

- 1 Gründer S & Pusch M (2015) Biophysical properties of acid-sensing ion channels (ASICs). *Neuropharmacology* **94**, 9–18.
- 2 Price MP, Snyder PM & Welsh MJ (1996) Cloning and expression of a novel human brain Na⁺ channel. *J Biol Chem* **271**, 7879–7882.
- 3 García-Añoveros J, Derfler B, Neville-Golden J, Hyman BT & Corey DP (1997) BNaC1 and BNaC2 constitute a new family of human neuronal sodium channels related to degenerins and epithelial sodium channels. *Proc Natl Acad Sci USA* **94**, 1459–1464.
- 4 Waldmann R, Champigny G, Bassilana F, Heurteaux C & Lazdunski M (1997) A proton-gated cation channel involved in acid-sensing. *Nature* **386**, 173–177.
- 5 Waldmann R & Lazdunski M (1998) H(+)-gated cation channels: neuronal acid sensors in the NaC/DEG family of ion channels. *Curr Opin Neurobiol* **8**, 418–424.
- 6 Paukert M, Sidi S, Russell C, Siba M, Wilson SW, Nicolson T & Gründer S (2004) A family of acid-sensing ion channels from the zebrafish: widespread expression in the central nervous system suggests a conserved role in neuronal communication. *J Biol Chem* **279**, 18783–18791.
- 7 Lin S-H, Sun W-H & Chen C-C (2015) Genetic exploration of the role of acid-sensing ion channels. *Neuropharmacology* **94**, 99–118.
- 8 Stewart AP, Haerteis S, Diakov A, Korbmacher C & Edwardson JM (2011) Atomic force microscopy reveals the architecture of the epithelial sodium channel (ENaC). *J Biol Chem* **286**, 31944–31952.

- 9 Lefèvre CMT, Diakov A, Haerteis S, Korbmacher C, Gründer S & Wiemuth D (2014) Pharmacological and electrophysiological characterization of the human bile acid-sensitive ion channel (hBASIC). *Pflugers Arch* **466**, 253–263.
- 10 Wiemuth D, Assmann M & Gründer S (2014) The bile acid-sensitive ion channel (BASIC), the ignored cousin of ASICs and ENaC. *Channels* **8**, 29–34.
- 11 Coric T, Zheng D, Gerstein M & Canessa CM (2005) Proton sensitivity of ASIC1 appeared with the rise of fishes by changes of residues in the region that follows TM1 in the ectodomain of the channel. *J Physiol* **568**, 725–735.
- 12 Coric T, Passamaneck YJ, Zhang P, Di Gregorio A & Canessa CM (2008) Simple chordates exhibit a proton-independent function of acid-sensing ion channels. *FASEB J* **22**, 1914–1923.
- 13 Canessa CM, Schild L, Buell G, Thorens B, Gautschi I, Horisberger JD & Rossier BC (1994) Amiloride-sensitive epithelial Na⁺ channel is made of three homologous subunits. *Nature* **367**, 463–467.
- 14 Lingueglia E, Voilley N, Waldmann R, Lazdunski M & Barbry P (1993) Expression cloning of an epithelial amiloride-sensitive Na⁺ channel. A new channel type with homologies to *Caenorhabditis elegans* degenerins. *FEBS Lett* **318**, 95–99.
- 15 Saxena A, Hanukoglu I, Strautnieks SS, Thompson RJ, Gardiner RM & Hanukoglu A (1998) Gene structure of the human amiloride-sensitive epithelial sodium channel beta subunit. *Biochem Biophys Res Commun* **252**, 208–213.
- 16 Voilley N, Bassilana F, Mignon C, Merscher S, Mattéi MG, Carle GF, Lazdunski M & Barbry P (1995) Cloning, chromosomal localization, and physical linkage of the beta and gamma subunits (SCNN1B and SCNN1G) of the human epithelial amiloride-sensitive sodium channel. *Genomics* **28**, 560–565.
- 17 Waldmann R, Champigny G, Bassilana F, Voilley N & Lazdunski M (1995) Molecular cloning and functional expression of a novel amiloride-sensitive Na⁺ channel. *J Biol Chem* **270**, 27411–27414.
- 18 Hanukoglu I & Hanukoglu A (2016) Epithelial sodium channel (ENaC) family: phylogeny, structure-function, tissue distribution, and associated inherited diseases. *Gene* **579**, 95–132.
- 19 Canessa CM, Merillat AM & Rossier BC (1994) Membrane topology of the epithelial sodium channel in intact cells. *Am J Physiol* **267**, C1682–C1690.
- 20 Chang SS, Grunder S, Hanukoglu A, Rösler A, Mathew PM, Hanukoglu I, Schild L, Lu Y, Shimkets RA, Nelson-Williams C *et al.* (1996) Mutations in subunits of the epithelial sodium channel cause salt wasting with hyperkalaemic acidosis, pseudohypoaldosteronism type 1. *Nat Genet* **12**, 248–253.
- 21 Edelheit O, Hanukoglu I, Gizewska M, Kandemir N, Tenenbaum-Rakover Y, Yurdakök M, Zajaczek S & Hanukoglu A (2005) Novel mutations in epithelial sodium channel (ENaC) subunit genes and phenotypic expression of multisystem pseudohypoaldosteronism. *Clin Endocrinol (Oxf)* **62**, 547–553.
- 22 Eastwood AL & Goodman MB (2012) Insight into DEG/ENaC channel gating from genetics and structure. *Physiology (Bethesda)* **27**, 282–290.
- 23 Zelle KM, Lu B, Pyfrom SC & Ben-Shahar Y (2013) The genetic architecture of degenerin/epithelial sodium channels in *Drosophila*. *G3: Genes - Genomes - Genetics*, **3**, 441–450.
- 24 Tavernarakis N & Driscoll M (1997) Molecular modeling of mechanotransduction in the nematode *Caenorhabditis elegans*. *Annu Rev Physiol* **59**, 659–689.
- 25 Holzer P (2015) Acid-sensing ion channels in gastrointestinal function. *Neuropharmacology* **94**, 72–79.
- 26 Enuka Y, Hanukoglu I, Edelheit O, Vaknine H & Hanukoglu A (2012) Epithelial sodium channels (ENaC) are uniformly distributed on motile cilia in the oviduct and the respiratory airways. *Histochem Cell Biol* **137**, 339–353.
- 27 Duc C, Farman N, Canessa CM, Bonvalet JP & Rossier BC (1994) Cell-specific expression of epithelial sodium channel alpha, beta, and gamma subunits in aldosterone-responsive epithelia from the rat: localization by in situ hybridization and immunocytochemistry. *J Cell Biol* **127**, 1907–1921.
- 28 Rossier BC, Baker ME & Studer RA (2015) Epithelial sodium transport and its control by aldosterone: the story of our internal environment revisited. *Physiol Rev* **95**, 297–340.
- 29 Garty H & Palmer LG (1997) Epithelial sodium channels: function, structure, and regulation. *Physiol Rev* **77**, 359–396.
- 30 Kellenberger S, Gautschi I & Schild L (1999) A single point mutation in the pore region of the epithelial Na⁺ channel changes ion selectivity by modifying molecular sieving. *Proc Natl Acad Sci USA* **96**, 4170–4175.
- 31 Friedlich AL (2012) Neocortical levels of lithium are increased in bipolar disorder. *Mol Psychiatry* **17**, 3–4.
- 32 Oruch R, Elderbi MA, Khattab HA, Pryme IF & Lund A (2014) Lithium: a review of pharmacology, clinical uses, and toxicity. *Eur J Pharmacol* **740**, 464–473.
- 33 Bassilana F, Champigny G, Waldmann R, De Weille JR, Heurteaux C & Lazdunski M (1997) The acid-sensitive ionic channel subunit ASIC and the mammalian degenerin MDEG form a heteromultimeric H⁺-gated Na⁺ channel with novel properties. *J Biol Chem* **272**, 28819–28822.
- 34 Sherwood TW, Lee KG, Gormley MG & Askwith CC (2011) Heteromeric acid-sensing ion channels (ASICs)

- composed of ASIC2b and ASIC1a display novel channel properties and contribute to acidosis-induced neuronal death. *J Neurosci* **31**, 9723–9734.
- 35 Li T, Yang Y & Canessa CM (2010) Leu85 in the beta1-beta2 linker of ASIC1 slows activation and decreases the apparent proton affinity by stabilizing a closed conformation. *J Biol Chem* **285**, 22706–22712.
- 36 Li T, Yang Y & Canessa CM (2010) Asn415 in the beta11-beta12 linker decreases proton-dependent desensitization of ASIC1. *J Biol Chem* **285**, 31285–31291.
- 37 Babini E, Paukert M, Geisler H-S & Grunder S (2002) Alternative splicing and interaction with di- and polyvalent cations control the dynamic range of acid-sensing ion channel 1 (ASIC1). *J Biol Chem* **277**, 41597–41603.
- 38 Chen X & Grunder S (2007) Permeating protons contribute to tachyphylaxis of the acid-sensing ion channel (ASIC) 1a. *J Physiol* **579**, 657–670.
- 39 Li T, Yang Y & Canessa CM (2012) Impact of recovery from desensitization on acid-sensing ion channel-1a (ASIC1a) current and response to high frequency stimulation. *J Biol Chem* **287**, 40680–40689.
- 40 Li T, Yang Y & Canessa CM (2010) Two residues in the extracellular domain convert a nonfunctional ASIC1 into a proton-activated channel. *Am J Physiol Cell Physiol* **299**, C66–C73.
- 41 Schuhmacher L-N, Srivats S & Smith ESJ (2015) Structural domains underlying the activation of acid-sensing ion channel 2a. *Mol Pharmacol* **87**, 561–571.
- 42 Kellenberger S & Schild L (2015) International union of basic and clinical pharmacology. XCI. structure, function, and pharmacology of acid-sensing ion channels and the epithelial Na⁺ channel. *Pharmacol Rev* **67**, 1–35.
- 43 Palmer LG, Patel A & Frindt G (2012) Regulation and dysregulation of epithelial Na⁺ channels. *Clin Exp Nephrol* **16**, 35–43.
- 44 Kashlan OB & Kleyman TR (2012) Epithelial Na⁺ channel regulation by cytoplasmic and extracellular factors. *Exp Cell Res* **318**, 1011–1019.
- 45 Horisberger JD & Chraïbi A (2004) Epithelial sodium channel: a ligand-gated channel? *Nephron Physiol* **96**, 37–41.
- 46 Bize V & Horisberger JD (2007) Sodium self-inhibition of human epithelial sodium channel: selectivity and affinity of the extracellular sodium sensing site. *Am J Physiol Renal Physiol* **293**, F1137–F1146.
- 47 Winarski KL, Sheng N, Chen J, Kleyman TR & Sheng S (2010) Extracellular allosteric regulatory subdomain within the gamma subunit of the epithelial Na⁺ channel. *J Biol Chem* **285**, 26088–26096.
- 48 Edelheit O, Ben-Shahar R, Dascal N, Hanukoglu A & Hanukoglu I (2014) Conserved charged residues at the surface and interface of epithelial sodium channel subunits—roles in cell surface expression and the sodium self-inhibition response. *FEBS J* **281**, 2097–2111.
- 49 Collier DM & Snyder PM (2009) Extracellular protons regulate human ENaC by modulating Na⁺ self-inhibition. *J Biol Chem* **284**, 792–798.
- 50 Sheng S, Maarouf AB, Bruns JB, Hughey RP & Kleyman TR (2007) Functional role of extracellular loop cysteine residues of the epithelial Na⁺ channel in Na⁺ self-inhibition. *J Biol Chem* **282**, 20180–20190.
- 51 Anantharam A, Tian Y & Palmer LG (2006) Open probability of the epithelial sodium channel is regulated by intracellular sodium. *J Physiol* **574**, 333–347.
- 52 Heidrich E, Carattino MD, Hughey RP, Pilewski JM, Kleyman TR & Myerburg MM (2015) Intracellular Na⁺ regulates epithelial Na⁺ channel maturation. *J Biol Chem* **290**, 11569–11577.
- 53 Jasti J, Furukawa H, Gonzales EB & Gouaux E (2007) Structure of acid-sensing ion channel 1 at 1.9 Å resolution and low pH. *Nature* **449**, 316–323.
- 54 Gonzales EB, Kawate T & Gouaux E (2009) Pore architecture and ion sites in acid-sensing ion channels and P2X receptors. *Nature* **460**, 599–604.
- 55 Dutertre S & Lewis RJ (2010) Use of venom peptides to probe ion channel structure and function. *J Biol Chem* **285**, 13315–13320.
- 56 Baron A, Diochot S, Salinas M, Deval E, Noël J & Lingueglia E (2013) Venom toxins in the exploration of molecular, physiological and pathophysiological functions of acid-sensing ion channels. *Toxicol* **75**, 187–204.
- 57 Chen X, Kalbacher H & Grunder S (2006) Interaction of acid-sensing ion channel (ASIC) 1 with the tarantula toxin psalmotoxin 1 is state dependent. *J Gen Physiol* **127**, 267–276.
- 58 Bacongus I & Gouaux E (2012) Structural plasticity and dynamic selectivity of acid-sensing ion channel-spider toxin complexes. *Nature* **489**, 400–405.
- 59 Dawson RJP, Benz J, Stohler P, Tetaz T, Joseph C, Huber S, Schmid G, Hügin D, Pflimlin P, Trube G *et al.* (2012) Structure of the acid-sensing ion channel 1 in complex with the gating modifier Psalmotoxin 1. *Nat Commun* **3**, 936.
- 60 Bacongus I, Bohlen CJ, Goehring A, Julius D & Gouaux E (2014) X-ray structure of acid-sensing ion channel 1-snake toxin complex reveals open state of a Na⁺-selective channel. *Cell* **156**, 717–729.
- 61 Kashlan OB & Kleyman TR (2011) ENaC structure and function in the wake of a resolved structure of a family member. *Am J Physiol Renal Physiol* **301**, F684–F696.
- 62 Brezovsky J, Chovancova E, Gora A, Pavelka A, Biedermannova L & Damborsky J (2013) Software

- tools for identification, visualization and analysis of protein tunnels and channels. *Biotechnol Adv* **31**, 38–49.
- 63 Masood TB, Sandhya S, Chandra N & Natarajan V (2015) CHEXVIS: a tool for molecular channel extraction and visualization. *BMC Bioinformatics* **16**, 119.
- 64 Kellenberger S, Hoffmann-Pochon N, Gautschi I, Schneeberger E & Schild L (1999) On the molecular basis of ion permeation in the epithelial Na⁺ channel. *J Gen Physiol* **114**, 13–30.
- 65 Kellenberger S, Auberson M, Gautschi I, Schneeberger E & Schild L (2001) Permeability properties of ENaC selectivity filter mutants. *J Gen Physiol* **118**, 679–692.
- 66 Chen J, Ray EC, Yates ME, Buck TM, Brodsky JL, Kinlough CL, Winarski KL, Hughey RP, Kleyman TR & Sheng S (2015) Functional roles of clusters of hydrophobic and polar residues in the epithelial Na⁺ channel knuckle domain. *J Biol Chem* **290**, 25140–25150.
- 67 Roy S, Boiteux C, Alijevic O, Liang C, Bernèche S & Kellenberger S (2013) Molecular determinants of desensitization in an ENaC/degenerin channel. *FASEB J* **27**, 5034–5045.
- 68 Springauf A, Bresenitz P & Gründer S (2011) The interaction between two extracellular linker regions controls sustained opening of acid-sensing ion channel 1. *J Biol Chem* **286**, 24374–24384.
- 69 Edelheit O, Hanukoglu I, Dascal N & Hanukoglu A (2011) Identification of the roles of conserved charged residues in the extracellular domain of an epithelial sodium channel (ENaC) subunit by alanine mutagenesis. *Am J Physiol Renal Physiol* **300**, F887–F897.
- 70 Paukert M, Chen X, Polleichtner G, Schindelin H & Gründer S (2008) Candidate amino acids involved in H⁺ gating of acid-sensing ion channel 1a. *J Biol Chem* **283**, 572–581.
- 71 Liechti LA, Berneche S, Bargeton B, Iwaszkiewicz J, Roy S, Michielin O & Kellenberger S (2010) A combined computational and functional approach identifies new residues involved in pH-dependent gating of ASIC1a. *J Biol Chem* **285**, 16315–16329.
- 72 Ishikita H (2011) Proton-binding sites of acid-sensing ion channel 1. *PLoS One* **6**, e16920.
- 73 Yang H, Yu Y, Li W-G, Yu F, Cao H, Xu T-L & Jiang H (2009) Inherent dynamics of the acid-sensing ion channel 1 correlates with the gating mechanism. *PLoS Biol* **7**, e1000151.
- 74 Li T, Youshan Y & Canessa CM (2009) Interaction of the aromatics Tyr-72/Trp-288 in the interface of the extracellular and transmembrane domains is essential for proton gating of acid-sensing ion channels. *J Biol Chem* **284**, 4689–4694.
- 75 Burley SK & Petsko GA (1985) Aromatic-aromatic interaction: a mechanism of protein structure stabilization. *Science* **229**, 23–28.
- 76 Sivasakthi V, Anitha P, Kumar KM, Bag S, Senthilvel P, Lavanya P, Swetha R, Anbarasu A & Ramaiah S (2013) Aromatic-aromatic interactions: analysis of π - π interactions in interleukins and TNF proteins. *Bioinformation* **9**, 432–439.
- 77 Sheng S, McNulty KA, Harvey JM & Kleyman TR (2001) Second transmembrane domains of ENaC subunits contribute to ion permeation and selectivity. *J Biol Chem* **276**, 44091–44098.
- 78 Sasaki S, Yui N & Noda Y (2014) Actin directly interacts with different membrane channel proteins and influences channel activities: AQP2 as a model. *Biochim Biophys Acta* **1838**, 514–520.
- 79 Li T, Yang Y & Canessa CM (2011) Outlines of the pore in open and closed conformations describe the gating mechanism of ASIC1. *Nat Commun* **2**, 399.
- 80 Sheng S, Li J, McNulty KA, Avery D & Kleyman TR (2000) Characterization of the selectivity filter of the epithelial sodium channel. *J Biol Chem* **275**, 8572–8581.
- 81 Sheng S, Perry CJ, Kashlan OB & Kleyman TR (2005) Side chain orientation of residues lining the selectivity filter of epithelial Na⁺ channels. *J Biol Chem* **280**, 8513–8522.
- 82 Li J, Sheng S, Perry CJ & Kleyman TR (2003) Asymmetric organization of the pore region of the epithelial sodium channel. *J Biol Chem* **278**, 13867–13874.
- 83 Snyder PM, Olson DR & Bucher DB (1999) A pore segment in DEG/ENaC Na(+) channels. *J Biol Chem* **274**, 28484–28490.
- 84 Fyfe GK, Zhang P & Canessa CM (1999) The second hydrophobic domain contributes to the kinetic properties of epithelial sodium channels. *J Biol Chem* **274**, 36415–36421.
- 85 Giraldez T, Rojas P, Jou J, Flores C & Alvarez de la Rosa D (2012) The epithelial sodium channel δ -subunit: new notes for an old song. *Am J Physiol Renal Physiol* **303**, F328–F338.
- 86 Zhao R-Z, Nie H-G, Su X-F, Han D-Y, Lee A, Huang Y, Chang Y, Matalon S & Ji H-L (2012) Characterization of a novel splice variant of δ ENaC subunit in human lungs. *Am J Physiol Lung Cell Mol Physiol* **302**, L1262–L1272.
- 87 Ji H-L, Zhao R-Z, Chen Z-X, Shetty S, Idell S & Matalon S (2012) δ ENaC: a novel divergent amiloride-inhibitable sodium channel. *Am J Physiol Lung Cell Mol Physiol* **303**, L1013–L1026.
- 88 García-Añoveros J, Ma C & Chalfie M (1995) Regulation of *Caenorhabditis elegans* degenerin proteins by a putative extracellular domain. *Curr Biol* **5**, 441–448.

- 89 Snyder PM, Bucher DB & Olson DR (2000) Gating induces a conformational change in the outer vestibule of ENaC. *J Gen Physiol* **116**, 781–790.
- 90 Adams CM, Price MP, Snyder PM & Welsh MJ (1999) Tetraethylammonium block of the BNC1 channel. *Biophys J* **76**, 1377–1383.
- 91 Waldmann R, Champigny G, Voilley N, Lauritzen I & Lazdunski M (1996) The mammalian degenerin MDEG, an amiloride-sensitive cation channel activated by mutations causing neurodegeneration in *Caenorhabditis elegans*. *J Biol Chem* **271**, 10433–10436.
- 92 Langloh AL, Berdiev B, Ji HL, Keyser K, Stanton BA & Benos DJ (2000) Charged residues in the M2 region of alpha-hENaC play a role in channel conductance. *Am J Physiol Cell Physiol* **278**, C277–C291.
- 93 Mähler J & Persson I (2012) A study of the hydration of the alkali metal ions in aqueous solution. *Inorg Chem* **51**, 425–438.
- 94 Kim DM & Nimigean CM (2016) Voltage-gated potassium channels: a structural examination of selectivity and gating. *Cold Spring Harb Perspect Biol* **8**, 1–20.
- 95 Roux B (2005) Ion conduction and selectivity in K(+) channels. *Annu Rev Biophys Biomol Struct* **34**, 153–171.
- 96 Noskov SY & Roux B (2006) Ion selectivity in potassium channels. *Biophys Chem* **124**, 279–291.
- 97 Catterall WA (2014) Structure and function of voltage-gated sodium channels at atomic resolution. *Exp Physiol* **99**, 35–51.
- 98 Payandeh J, Scheuer T, Zheng N & Catterall WA (2011) The crystal structure of a voltage-gated sodium channel. *Nature* **475**, 353–358.
- 99 Zhou Y, Morais-Cabral JH, Kaufman A & MacKinnon R (2001) Chemistry of ion coordination and hydration revealed by a K⁺ channel-Fab complex at 2.0 Å resolution. *Nature* **414**, 43–48.
- 100 Naylor CE, Bagnéris C, DeCaen PG, Sula A, Scaglione A, Clapham DE & Wallace BA (2016) Molecular basis of ion permeability in a voltage-gated sodium channel. *EMBO J* **35**, 820–830.
- 101 Lai HC & Jan LY (2006) The distribution and targeting of neuronal voltage-gated ion channels. *Nat Rev Neurosci* **7**, 548–562.
- 102 De Lera Ruiz M & Kraus RL (2015) Voltage-gated sodium channels: structure, function, pharmacology, and clinical indications. *J Med Chem* **58**, 7093–7118.
- 103 Ahern CA, Payandeh J, Bosmans F & Chanda B (2016) The hitchhiker's guide to the voltage-gated sodium channel galaxy. *J Gen Physiol* **147**, 1–24.
- 104 Corry B & Thomas M (2012) Mechanism of ion permeation and selectivity in a voltage gated sodium channel. *J Am Chem Soc* **134**, 1840–1846.
- 105 Yang L & Palmer LG (2014) Ion conduction and selectivity in acid-sensing ion channel 1. *J Gen Physiol* **144**, 245–255.
- 106 Hanukoglu A, Edelheit O, Shriki Y, Gizewska M, Dascal N & Hanukoglu I (2008) Renin-aldosterone response, urinary Na/K ratio and growth in pseudohypoaldosteronism patients with mutations in epithelial sodium channel (ENaC) subunit genes. *J Steroid Biochem Mol Biol* **111**, 268–274.
- 107 Edelheit O, Hanukoglu I, Shriki Y, Tfilin M, Dascal N, Gillis D & Hanukoglu A (2010) Truncated beta epithelial sodium channel (ENaC) subunits responsible for multi-system pseudohypoaldosteronism support partial activity of ENaC. *J Steroid Biochem Mol Biol* **119**, 84–88.